

GA-A26730

PULSE-DILATION ENHANCED GATED OPTICAL IMAGER WITH 5 ps RESOLUTION

by

T.J. HILSABECK, J.D. KILKENNY, J.D. HARES,
A.K.L. DYMOKE-BRADSHAW, P.M. BELL, J.A. KOCH,
P.M. CELLIERS, D.K. BRADLEY, T. McCARVILLE,
M. PIVOVAROFF, R. SOUFLI and R. BIONTA

JUNE 2010



DISCLAIMER

This report was prepared as an account of work sponsored by an agency of the United States Government. Neither the United States Government nor any agency thereof, nor any of their employees, makes any warranty, express or implied, or assumes any legal liability or responsibility for the accuracy, completeness, or usefulness of any information, apparatus, product, or process disclosed, or represents that its use would not infringe privately owned rights. Reference herein to any specific commercial product, process, or service by trade name, trademark, manufacturer, or otherwise, does not necessarily constitute or imply its endorsement, recommendation, or favoring by the United States Government or any agency thereof. The views and opinions of authors expressed herein do not necessarily state or reflect those of the United States Government or any agency thereof.

PULSE-DILATION ENHANCED GATED OPTICAL IMAGER WITH 5 ps RESOLUTION

by

T.J. HILSABECK, J.D. KILKENNY, J.D. HARES,*
A.K.L. DYMOKE-BRADSHAW,* P.M. BELL,† J.A. KOCH,†
P.M. CELLIERS,† D.K. BRADLEY,† T. McCARVILLE,†
M. PIVOVAROFF,† R. SOUFLI† and R. BIONTA†

This is a preprint of an invited paper to be presented at the
18th Topical Conference on High Temperature Plasma
Diagnostics, May 16–20, 2010 in Wildwood, New Jersey and
to be published in Review of Scientific Instruments.

*Kentech Instruments Ltd.

†Lawrence Livermore National Laboratory, Livermore, California

Work supported in part by
the U.S. Department of Energy
under DE-AC05-07NA27344 and
General Atomics Internal Funding

GENERAL ATOMICS ATOMICS PROJECT 40011
JUNE 2010



ABSTRACT

A 5 ps gated framing camera was demonstrated using the pulse-dilation of a drifting electron signal. The pulse-dilation is achieved by accelerating a photoelectron derived information pulse with a time varying potential [R.D. Prosser, J. Phys. E **9**, 57 (1976)]. The temporal dependence of the accelerating potential causes a birth time dependent axial velocity dispersion that spreads the pulse as it transits a drift region. The expanded pulse is then imaged with a conventional gated micro-channel plate based framing camera and the effective gating time of the combined instrument is reduced over that of the framing camera alone. In the drift region, electron image defocusing in the transverse or image plane is prevented with a large axial magnetic field. Details of the unique issues associated with rf excited photocathodes were investigated numerically and a prototype instrument based on this principle was recently constructed. Temporal resolution of the instrument was measured with a frequency tripled femtosecond laser operating at 266 nm. The system demonstrated 20X temporal magnification and the results are presented here. X-ray image formation strategies and photometric calculations for ICF implosion experiments are also examined.

I. INTRODUCTION

Framing cameras are used to assess the symmetry of imploding targets in laser driven inertial confinement fusion experiments. Fast gate times are needed to avoid motional blurring due to the high velocities and small spatial dimensions of the imploding targets. High speed image gating is accomplished by energizing a photomultiplier array of microchannel pores with a high voltage, short duration electrical pulse.¹ Photons incident on the front surface of the array generate electrons which are accelerated through the microchannel pores by the high electric field. As a result of collision with the pore walls, secondary electrons are liberated in this process and the device produces gain. The lower limit on the gate time achievable with such a device is related to the transit time of electrons through the microchannel plate pores. Using thin substrates, FWHM temporal gate times as low as 30 ps have been achieved.² However, further reductions in gate times via this approach are impractical due to the loss of gain and increased fragility of the detector.

An alternate approach to obtaining shorter gate widths is arrived at by decoupling the photoelectron production and the gain producing photomultiplier array. The electron signal may then be manipulated with electromagnetic fields in a vacuum drift region prior to its arrival at the microchannel plate. In particular, the electron pulse generated at the photocathode may be accelerated by a time varying electric field in such a manner that the initial electrons transit the drift region at a higher velocity than those coming later. Thus, the temporal shape of the information signal arriving at the photomultiplier array will be dilated or temporally magnified with respect to the photon signal incident on the cathode as depicted in Fig. 1. Pulse-dilation was used to reduce the necessary bandwidth of an oscilloscope used to observe fast transient electrical signals³ and axial magnetic fields have been used to store images created from photoelectron emission in several applications.^{4,5} Here, we combine these techniques in order to achieve extremely fast electrical gating of two dimensional images.

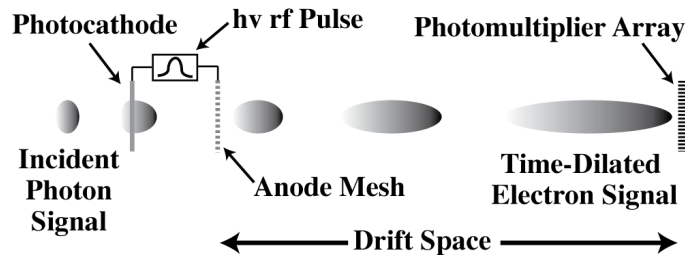


FIG. 1. Principle of pulse-dilation: photoelectrons are accelerated with a time varying electric field and the resulting energy dispersion causes the signal to stretch axially as it traverses the drift region resulting in reduced effective temporal resolution when sampled with a gated microchannel plate.

II. DESIGN CONSIDERATIONS AND ANALYSIS

The temporal magnification of an incident signal depends upon the temporal profile of the photocathode excitation pulse and the length of the drift region. Consider two photoelectrons which enter the drift region at times t_0 and t_1 . In the limit of small accelerating gap and ignoring any birth energy spread, the kinetic energy of the electrons will be given by the cathode-anode potential difference and they will exit the drift region at time

$$t'_i = L \sqrt{\frac{m}{2e\phi(t_i)}} + t_i \quad . \quad (1)$$

Here, m is the electron mass, $e > 0$ is the magnitude of the electron charge, L is the length of the drift region, $\phi(t)$ is the cathode-anode difference potential and $i = 0, 1$ indexes the particles. We may associate a temporal magnification factor

$$m(t_1, t_0) = \frac{t'_1 - t'_0}{t_1 - t_0} \approx 1 + \frac{L}{2v_d} \frac{|\dot{\phi}|}{\phi} \quad , \quad (2)$$

with respect to the difference in arrival times of the two electrons where v_d is the average velocity for electrons in the signal pulse transiting the drift region. Figure 2 shows the resultant temporal magnification for the specific case where the cathode-anode potential difference decays linearly from -5 kV to ground in 500 ps, $t_1 - t_0 = 10$ ps and $L = 50$ cm. At 100 ps, cathode-anode potential has fallen to -4 kV and the temporal magnification is 17. These conditions represent the design point for the instrument discussed below.

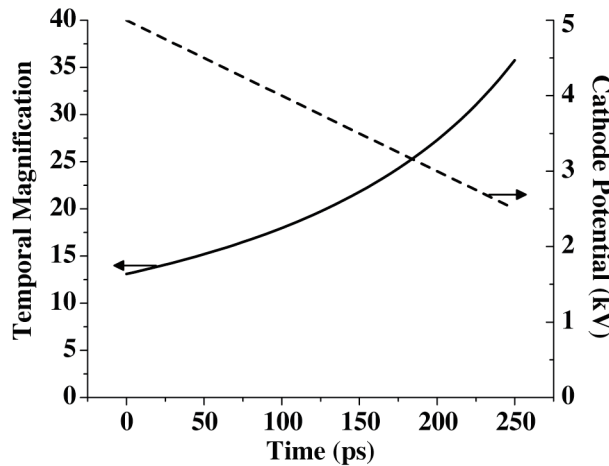


FIG. 2. Temporal magnification of a 10 ps signal when accelerated by a -10 V/ps potential ramp and drifting over a 50 cm length.

In reality, photoelectrons are born with a range of initial energies represented by a temperature, and the electric fields in the accelerating gap are finite. These conditions

introduce a limit to the minimum achievable temporal resolution of the device. An electron born slightly later with higher initial energy can catch up to an electron born earlier with lower energy. Thus, the temporal causality of the electron source process or input signal is spoiled. In order to estimate the magnitude of this effect, a one dimensional numerical simulation of the acceleration process for electrons born with differing initial energy spreads was performed. An ensemble of electrons are sourced at the photocathode with a range of initial velocities based on the temperature distribution and their motion through the accelerating gap and down the drift tube is followed. The acceleration gap was 1.6 mm, the drift region 50 cm and the drift energy approximately 4 keV. A comparison of two output signals is shown in Fig. 3. In each case the input signal was two Gaussian pulses of width 1 ps with their peaks separated by 6 ps. The black curve represents the output signal for the case in which all electrons are born with no initial kinetic energy. For the gray curve, the electron birth energy is normally distributed with a temperature of 1 eV. Under these conditions, the width of the output signal is just starting to be impacted.

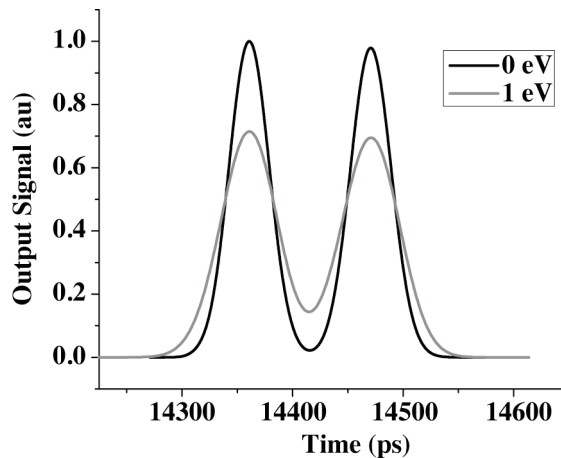


FIG. 3. Comparison of pulse-dilated output signals showing the broadening effect caused by finite photoelectron birth energy spread. In each case, the input signal consisted of two 1 ps wide Gaussian pulses separated by 6 ps.

Another possible limitation to the temporal resolution is space charge repulsion. At sufficiently high photocurrent density, electric fields produced by the electrons themselves can lead to modifications of the particle trajectories. In our device, the dominant effect will occur for motion in the drift direction due to the presence of a large axial magnetic field.

Space charge repulsion will cause additional spreading of the electron signal beyond that expected due to pulse-dilation. The photocurrent density at which space charge effects will begin to affect the output signal was obtained via particle-in-cell simulation. For this work, a 2D axisymmetric OOPIC (object oriented particle in cell) code was employed.⁴ A Gaussian photocurrent pulse of width 1 ps was emitted from a 1 cm² circular region of the cathode. The cathode potential was ramped to ground from -5 kV over a 500 ps period and

the photocurrent pulse emission peaked at -4 kV. A large axial magnetic field was included in the simulation to avoid transverse pulse spreading. The PIC simulation was continued until all electrons left the accelerating gap and entered the field free region approximately 1 cm past the anode mesh. The particle positions and velocities were then output from the simulation and the signal arrival time at the end of a 50 cm drift region was calculated. Figure 4 shows the width of the output signal as a function of the peak photocurrent emission density. At low currents, the signal width is constant and very close to the value predicted in Fig. 2. At a peak emission photocurrent density of 1 mA/mm^2 , the output signal pulse width begins to increase. This level corresponds to approximately one electron emitted per picosecond per $160 \text{ }\mu\text{m}^2$ area.

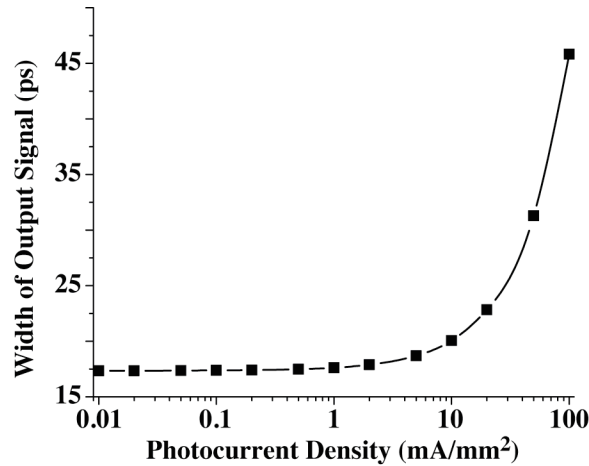


FIG. 4. PIC calculations of pulse broadening due to space charge repulsion of the photoelectrons. The input signal was a 1 ps wide Gaussian pulse with peak photocurrent density given on the abscissa.

A large uniform axial magnetic field is provided to prevent the electrons from spreading out in the transverse direction causing image defocusing. Thus, the electrons execute cyclotron motion as they transit the drift space. The radial extent of this motion sets the minimum spatial resolution achievable in the device. Image blurring due to electron cyclotron motion occurs over a distance of $4 r_c = 9.5 T_{\perp}^{1/2} / B \text{ }\mu\text{m}$, where T_{\perp} is the transverse electron kinetic energy in eV and B is the magnetic field strength in Tesla. The minimum transverse electron kinetic energy is given by the spread in photoelectron birth energy and is typically on the order of 1 eV. However, additional contributions can occur if there are appreciable transverse electric fields in the accelerating region. Therefore, it is necessary to ensure that the photocathode and anode mesh planes are normal to the focusing magnetic field direction and to avoid generating photoelectrons near the fringing fields near the edges of the photocathode conducting surfaces. There are two secular drifts associated with electron motion in non-uniform magnetic fields. The first arises due to gradients in the magnetic field strength and is approximately given by $x_{\nabla B} = Lv_{\perp}^2 / \omega_c v_{\parallel} \delta$ where ω_c is the angular frequency of the cyclotron motion, δ is the scale length over which the magnetic

field changes, L is the length of the drift region, v_{\perp} is the electron velocity perpendicular to the magnetic field direction and v_{\parallel} is the velocity of the electron's guiding center along the magnetic field direction. For the instrument discussed here, this drift is sub-micron in length. The second secular drift is due to the curvature of magnetic field lines and is proportional to the parallel energy of the electrons. The magnitude of the curvature drift may be approximated as $x_{curv} = Lv_{\parallel}^2 / \omega_c R_c$ where R_c is the radius of curvature for the magnetic field line. Since the parallel velocity is large, the curvature drift can be significant in cases where the direction of the magnetic field lines changes appreciably. However, all of the particles will experience an approximately equal drift displacement and as a result image blurring is not incurred. There is a relative drift due to the parallel velocity dispersion necessary for pulse-dilation, but it is negligible in all but the most extreme cases.

Several interesting phenomena associated with rf excited photocathodes affect the operation of the pulse-dilation imaging system. In the first case, the time varying nature of the accelerating field causes a temporal dispersion of the output signal across the image plane. This may be understood as a finite wavelength effect inherent in the rf excitation of the photocathode. This phenomenon is absent for static potentials used in conventional streak camera designs, although significant time dispersion across the cathode can originate from a change in the cathode to deflection plate transit time as one moves off axis and curved streaks may appear at high streak speeds. To calculate the magnitude of the finite wavelength effect, a full-wave electromagnetic simulation of the photocathode charging was performed. The results indicate that at a particular instant during the ramp at which time the acceleration potential is approximately 4150 V there is a potential variation of approximately 48 V across a 5 mm diameter circular region centered on the cathode. With a 10V/ps potential ramp, this variation corresponds to an effective temporal spread of approximately 5 ps. This example illustrates a system design constraint wherein the requirements for temporal resolution and image plane aperture size limit the rate at which the accelerating potential may be ramped and sets the maximum temporal magnification per unit drift length of the instrument.

The second important observation concerning rf excitation of the photocathode involves the magnetic field component of the electromagnetic wave. For the high accelerating fields used in this device, the magnetic field component can be several tens of gauss. Since the direction of this rf magnetic field is transverse to the accelerating electric field, it effectively changes the magnetic field direction during the acceleration time which would result in a transverse energy component in the electron signal. In order to avoid this deleterious situation, the rf magnetic field component must be reduced. One method of achieving this is to counter propagate another wave in the opposite direction with the appropriate phase and polarization. It is possible to arrange the waves such that the electric field components add whereas the magnetic field components cancel. A simple method for achieving this cancellation is to form a transmission line open near the active region of the photocathode. The incident wave reflects back onto itself in the desired phase to cancel the magnetic field

while reinforcing the electric field. Another possibility is to excite the photocathode with colliding pulses from a dual feed arrangement. Figure 5 shows the rf magnetic field strength in the accelerating gap of the photocathode for three different excitation scenarios. In each case, a peak accelerating field of 3 kV/mm is reached in the accelerating gap. For the straight transmission line, the rf magnetic field strength exceeds 100 Gauss and would result in significant transverse energy excitation. Fortunately, the open reflection and colliding pulse arrangements substantially reduce the rf magnetic field to acceptable levels for good spatial resolution. Another strategy for eliminating rf magnetic field is to superimpose an rf excitation pulse with zero net current at the gating time onto a static DC voltage. This can be accomplished by capacitively coupling the rf transmission line to the photocathode strip. This configuration allows a single gate pulse to transit a large photocathode area and provide gating for multiple frames.

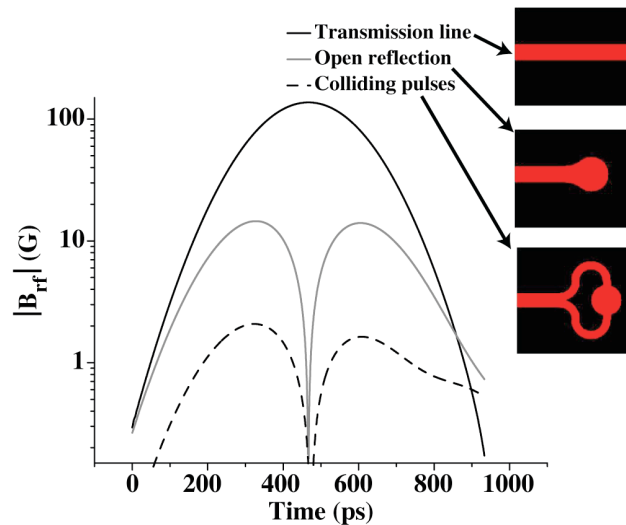


FIG. 5. RF magnetic field component taken from an electromagnetic simulation of the excitation for three different photocathode designs. Input strip widths are 5 mm and circular cathode diameters are 10 mm. In each case, the electric field strength peaked at 30 kV/cm in the cathode center. It is necessary to reduce the rf component of the magnetic field in order to avoid large transverse energy excitation and reduced spatial resolution in the electron images.

III. INSTRUMENT DESIGN

A prototype instrument has been constructed to demonstrate the principle of using pulse-dilation to achieve very fast gating of a two dimensional image. The photocathode was constructed from a 2-in. diameter fused silica window coated with 100 nm of Au. A 1.6 mm accelerating gap was formed between the photocathode and an electroformed 500 lines per inch nickel mesh held at ground. The photocathode was excited from a 50 Ω microstrip transmission line printed on RT 5880 Duroid substrate. The excitation pulse was formed by a Kentech PBG1 based pulser and built up to -3 kV over 100 ps and then decayed roughly linearly to ground over 500 ps. Simulation results showed that the pulse reflection at the photocathode resulted in a peak voltage of -5 kV and that at the target drift energy of -4 keV, the potential was changing at approximately -10 V/ps. The drift distance from the anode mesh to the microchannel plate detector was 50 cm. Calculations show that these conditions produce a temporal magnification of approximately 17X. A magnetic focusing field of 400 gauss was produced with four 40 cm diameter coils. Each coil has an axial length of 8 cm and they are spaced with a 15 cm gap between them. A photograph of the instrument is shown in Fig. 6. The vacuum chamber is a 4-in. diameter tube of 316 stainless and is evacuated with a 300 l/s turbo-molecular pump. The system achieved an operating pressure below 10^{-5} Torr. The pulse-dilated electron signal was gated with the Flexible X-ray Imager (FXI) microchannel plate detector on loan from LLNL. The measured gate width of the FXI instrument is approximately 80 ps.⁵

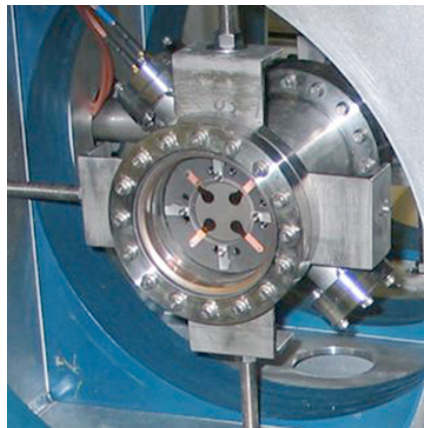


FIG. 6. Front end view of the pulse-dilation instrument. Four 10 mm diameter photocathodes are visible in the center of the viewport. The vacuum tube is centered on the axis of the blue magnet coils. Photocathode pulser excitation enters through coaxial feedthroughs entering from the upper left.

IV. EXPERIMENTAL DEMONSTRATION

The temporal resolution of the pulse-dilation enhanced FXI instrument was characterized using 100 fs ultraviolet (uv) light pulses obtained by frequency tripling the output of a Quantronix Integra-C Ti-Sapphire laser system. During the experiments, the laser system provided approximately 1 mJ pulses at 800 nm. The fundamental frequency pulses were passed through the Quantronix STHG-400/266 harmonic generator module which output approximately 80 μ J at 266 nm. The laser system was operating at a repetition rate of 500 Hz. The uv pulse was sent through an 80 ns optical delay line formed using 12 dielectric mirrors arranged on the optical table. The optical delay is necessary to allowing adequate time for the triggering of the photocathode and FXI pulsers. The uv light pulse was then passed through a Mach-Zehnder interferometer which output a pair of pulses. A mirror in one leg of the interferometer was mounted on an adjustable stage so that the relative temporal spacing of the pulses could be continuously varied. Each leg of the interferometer contained an aperture in the shape of an arrow which was imaged onto the photocathode of the pulse-dilation instrument using a lens placed at the output of the interferometer. The arrow aperture in the fixed length leg of the interferometer was pointing in a direction parallel to the plane of the optical table, whereas the arrow in the variable length leg was pointing in the vertical direction. The two distinguishable apertures allowed unambiguous identification of the light pulses in the output images of the instrument. Triggering of the photocathode and FXI pulsers was accomplished utilizing the 400 nm light pulse that is also output by the harmonic generation module. The 400 nm pulse was focused onto a photodiode of approximately 0.2 ns rise time. The photodiode output was then sent to a trigger discriminator circuit which amplified the photodiode signal and reduced the repetition rate to 50 Hz. A schematic diagram of the complete experimental setup is given in Fig. 7.

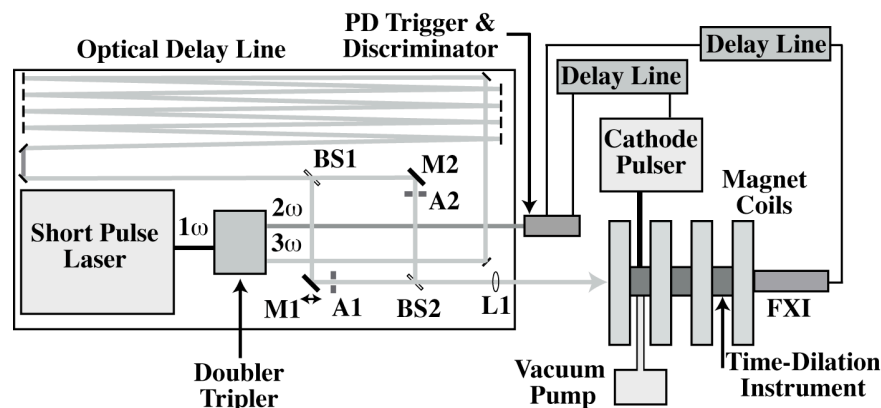


FIG. 7. Experimental setup used in the pulse-dilation demonstration. (left) Optics table used to produce a pair of 100 fs uv light pulses. (right) Pulse-dilation instrument components and trigger delay lines.

In order to produce the desired pulse-dilation factor in the drifting electron signal, the arrival of the photon signal at the photocathode must coincide with a specific voltage level

(and slope) of the rf excitation delivered by the pulser. Additionally, the gating of the microchannel plate detector at the end of the drift region must coincide with the arrival of the pulse-dilated electron pulse. These timing conditions were obtained in the following manner. First, the photocathode was biased to -700 VDC. Next, the uv pulse traversing the fixed length leg of the interferometer (horizontal arrow) was imaged onto the photocathode (vertical arrow blocked). The triggering of the FXI gate was then adjusted using variable length cables so that the horizontal arrow image was visible on the output phosphor. The triggering of the FXI gate was then adjusted by a calculated amount to the time expected for the arrival of electrons accelerated by a -4 kV potential. The photocathode was then excited by the time varying potential from the hv pulser. The trigger signal to the pulser was adjusted using a Kentech programmable delay line (25 ps steps) and a continuously variable trombone section of transmission line until the horizontal arrow reappeared at the output phosphor. Under these conditions, the instrument is properly timed.

To measure the temporal response of the instrument, the variable length leg of the interferometer was unblocked and the vertical arrow was imaged onto the photocathode. The optical path length of the vertical arrow uv pulse was adjusted in small steps and a number of output images were captured at each setting. This procedure was repeated until the vertical arrow appeared and then disappeared from the output image. Figure 8 shows six output images obtained from this experiment. Under each image is the relative change in the optical path traversed by the vertical arrow pulse along with the associated time delay. The vertical arrow appears and then disappears over a temporal delay adjustment of ~ 5 ps. A schematic representation of the instrument gating condition is shown above each image. The white triangle represents the temporal period over which the instrument gate is open. The horizontal arrow arrival time is fixed and centered within the instrument gating interval as evidenced by its continuous appearance in each image. The arrival time of the vertical arrow is changing as its optical path length is varied and it is swept through the gating interval of the instrument resulting in its appearance and subsequent disappearance from the images. The length of the arrows in Fig. 8 is approximately 4 mm.

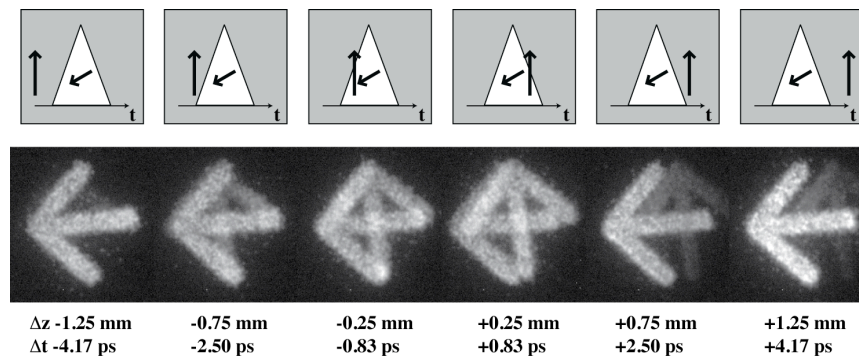


FIG. 8. Demonstration of pulse-dilation imaging. Six image frames are shown along with associated vertical arrow interferometer path length setting. While timing is set to image horizontal arrow, vertical arrow comes into and recedes from view when optical path is varied by 1.5 mm indicating a 5 ps gate width. Depiction of the gating condition for each image shown above the images.

V. PROSPECTS FOR ICF DIAGNOSTICS

Pulse-dilation provides a method for obtaining two dimensional images with gate times on the order of several picoseconds. Possible uses for this technology include: measuring high energy electron transport rates in fast ignition experiments, analyzing the symmetry of late stage implosion of high energy targets and burn wave dynamics for igniting targets. In each case, it will be necessary to image the hard x-ray emission source. The pinhole is a commonly used x-ray image formation device. However, the pinhole diameter must be small in order to achieve good spatial resolution and the light gathering efficiency is correspondingly limited. Consider an emission source of 10^{15} W/cm² sr keV centered around 10 keV and suppose we are interested in obtaining images with 5 ps gate times through a 10 μ m pinhole over a 1 keV energy range. The number of photons per resolution element arriving at the detector is approximately $1.9 \times 10^6 / p^2$ where p is the pinhole-source distance in centimeters. For a photocathode with 1% quantum efficiency for secondary electron emission, the pinhole must be no further than 5 cm from the target in order to allow the signal-to-noise ratio to reach 30. Primary photoelectrons, which are emitted from the photocathode with kinetic energies significantly higher than a few electron volts, are not resolved either temporally or spatially by the device and represent a background signal in the image.

In some experiments, pinhole imaging may not provide adequate signal intensity to the imager due to low source brightness or a limitation on the minimum pinhole to target separation distance. An alternative imaging approach with higher collection efficiency and reduced geometric constraints uses a Kirkpatrick-Baez (KB) microscope that forms x-ray images using a pair of grazing incidence mirrors. A KB microscope imaging system is a potential candidate for use at the National Ignition Facility during experiments on igniting capsules when neutron production is expected to be large.

In order to shield the image recording electronics from excess noise due to neutron irradiation, it will be necessary to position the pulse-dilation instrument behind the 2 m thick target chamber wall, 19 m from the target chamber center. The KB mirrors are positioned inside the target chamber at 1.5 m giving an approximate system magnification of 12. The focusing mirror surfaces must be elliptically figured to provide resolution better than 10 μ m; the on-axis resolution can be considerably better than this, but obliquity will limit the off-axis resolution especially near the edge of the field of view.⁶ The required mirror figure accuracy was investigated analytically using the ray tracing program ZEMAX. For analysis, the mirrors were approximately 200 mm in length and operating at a grazing angle of 0.75 deg. The elliptical mirror shapes were approximated with polynomials and the point spread functions were examined for various levels of figure error. The results indicate that an aspheric figure error of <2 nm rms yields 5 μ m spatial resolution over a 150 μ m object plane field of view. A conceptual design of the mirror system was completed and it was found that

contributions to figure error from gravity sag, mounting stresses, manufacturing tolerances and coating non-uniformity can each be reduced to approximately the 1 nm level.

Fabricating the high collection efficiency optics that satisfy the stringent manufacturing tolerances necessary for picoseconds range image gating is costly. Accordingly, it will be desirable to obtain multiple frames from each image. Since the hard x-rays are not appreciably absorbed in one pass through the transmission photocathode, it is possible to use the image repeatedly by arranging for the x-ray signal to intersect a group of transmission photocathodes. The magnetic axis of the pulse-dilation instrument may be angled with respect to the incident direction of the x-rays. The excitation pulse of each photocathode may be timed independently so that the timing of the frame is also independent and a time series of frames from a single line of sight image view may be obtained.

REFERENCES

- ¹J. D. Kilkenny, *Laser Part. Beams* **9**, 49 (1991).
- ²D. K. Bradley, P. M. Bell, O. L. Landen, J. D. Kilkenny, and J. Oertel, *Rev. Sci. Instrum.* **66**, 716 (1995).
- ³R. D. Prosser, *J. Phys. E* **9**, 57 (1976).
- ⁴J. D. McGee, J. Beesley and A. D. Berg, *J. Sci. Instrum.* **43**, 153 (1966).
- ⁵J. P. Fabre, S. V. Golovkin, A. E. Kushnirenko, A. M. Medvedkov, E. N. Kozarenko, I. E. Kreslo, A. G. Berkovski, Y. I Gubanov, G. N. Kislizkaya, G. Chiodi, A. Frenkel, G. Martellotti, D. Mazza and G. Penso, *Proc. SPIE* **2549**, 46 (1995).
- ⁶J. P. Verboncoeur, A. B. Langdon, and N. T. Gladd, *Comp. Phys. Comm.* **87**, 199 (1995).
- ⁷K. S. Budil, T. S. Perry, P. M. Bell, J. D. Hares, P. L. Miller, T. A. Peyser, R. Wallace, H. Louis, and D. E. Smith, *Rev. Sci. Instrum.* **485**, 199 (1996).
- ⁸J. A. Koch, O. L. Landen, J. T. W. Barbee, P. Celliers, L. B. D. Silva, S. G. Glendinning, B. A. Hammel, D. H. Kalantar, C. Brown, J. Seely, G. R. Bennet and W. Hsing, *Appl. Opt.* **37**, 1784 (1998).

ACKNOWLEDGMENT

Many useful discussions were held with colleagues at LLNL including: M. Eckart, O. Landen, P. Springer, R. Shepherd, A. McPhee and C. Halvorson. Appreciation is also due to E. Lundgren, A. Clark, A. Forsman and C. Moeller for their help in constructing the instrument and setting up the test facility at General Atomics. This work supported in part by General Atomics internal funding and Kentech Instruments Ltd. internal funding. Lawrence Livermore National Laboratory is operated by Lawrence Livermore National Security, LLC, for the U.S. Department of Energy, National Nuclear Security Administration under Contract DE-AC52-07NA27344.